Hindawi Publishing Corporation
Advances in High Energy Physics
Volume 2016, Article ID 1903767, 8 pages
http://dx.doi.org/10.1155/2016/1903767

Research Article

Shell Model Studies of Competing Mechanisms to the Neutrinoless Double-Beta Decay in ^{124}Sn, ^{130}Te, and ^{136}Xe

Andrei Neacsu and Mihai Horoi

Department of Physics, Central Michigan University, Mount Pleasant, MI 48859, USA

Correspondence should be addressed to Andrei Neacsu; neacs1a@cmich.edu

Received 29 June 2016; Accepted 8 September 2016

Academic Editor: Theocharis Kosmas

Neutrinoless double-beta decay is a predicted beyond Standard Model process that could clarify some of the not yet known neutrino properties, such as the mass scale, the mass hierarchy, and its nature as a Dirac or Majorana fermion. Should this transition be observed, there are still challenges in understanding the underlying contributing mechanisms. We perform a detailed shell model investigation of several beyond Standard Model mechanisms that consider the existence of right-handed currents. Our analysis presents different venues that can be used to identify the dominant mechanisms for nuclei of experimental interest in the mass $A \sim 130$ region (^{124}Sn, ^{130}Te, and ^{136}Xe). It requires accurate knowledge of nine nuclear matrix elements that we calculate in addition to the associated energy-dependent phase space factors.

1. Introduction

Should the neutrinoless double-beta decay ($0\nu\beta\beta$) be experimentally observed, the lepton number conservation is violated by two units and the back-box theorems [1–4] predict the neutrino to be a Majorana particle. In addition to the nature of the neutrino (whether a Dirac or a Majorana fermion), there are other unknown properties of the neutrino that could be investigated via $0\nu\beta\beta$, such as the mass scale, the absolute mass, or the underlying neutrino mass mechanism. There are several beyond Standard Model mechanisms that could compete and contribute to this process [5, 6]. Reliable calculations of the nuclear matrix elements (NME) are necessary to perform an appropriate analysis that could help evaluate the contribution of each mechanism.

The most commonly investigated neutrinoless $0\nu\beta\beta$ mechanism is the so-called mass mechanism involving the exchange of light left-handed neutrinos, for which the NME were calculated using many nuclear structure methods. Calculations that consider the contributions of heavy, mostly sterile, right-handed neutrinos have become recently available, while left-handed heavy neutrinos have been shown to have a negligible effect [7, 8] and their contribution is generally dismissed. A comparison of the recent mass mechanism results obtained with the most common methods can be seen in Figure 6 of [9], where one can notice the differences that still exist among these nuclear structure methods. Figure 7 of [9] shows the heavy neutrino results for several nuclear structure methods, and the differences are even larger than those in the light neutrino case because of the uncertainties related to the short-range correlation (SRC) effects. There are efforts to reduce these uncertainties by the development of an effective transition operator that treats the SRC consistently [10].

Because shell model calculations were successful in predicting two-neutrino double-beta decay half-lives [11] before experimental measurements and as shell model calculations of different groups largely agree with each other without the need to adjust model parameters, we calculate our nuclear matrix elements using shell model techniques and Hamiltonians that reasonably describe the experimental spectroscopic observables.

Experiments such as SuperNEMO [12, 13] could track the outgoing electrons and help distinguish between the mass mechanism (ν) and so-called λ and η mechanisms [14, 15]. This would also provide complementary data at low energies for testing the existence of right-handed contributions predicted by left-right symmetric models [15–19], currently

investigated at high energies in colliders and accelerators such as LHC [20]. To distinguish the possible contribution of the heavy right-handed neutrino using shell model nuclear matrix elements, measurements of lifetimes for at least two different isotopes are necessary, ideally that of an $A \sim 80$ isotope and another lifetime of an $A \sim 130$ isotope, as discussed in Section V of [21]. It is expected that if the neutrinoless double-beta decay is confirmed in any of the experiments, more resources and upgrades could be dedicated to boost the statistics and to reveal more information on the neutrino properties.

Following our recent study for ^{82}Se in [21], which is the baseline isotope of SuperNEMO, we extend our analysis of λ and η mechanisms to other nuclei of immediate experimental interest: ^{124}Sn, ^{130}Te, and ^{136}Xe. These isotopes are under investigation by the TIN.TIN [22] (^{124}Sn), CUORE [23, 24], SNO+ [25] (^{130}Te), NEXT [26], EXO [27], and KamLAND-Zen [28] (^{136}Xe) experiments. For the mass region $A \sim 130$, we perform calculations in $jj55$ model space consisting of $0g_{7/2}, 1d_{5/2}, 1d_{3/2}, 2s_{1/2}$ and $0h_{11/2}$ valence orbitals using the SVD shell model Hamiltonian [29] that was fine-tuned with experimental data from Sn isotopes. Our tests of this Hamiltonian include energy levels, $B(E2)\uparrow$ transitions, occupation probabilities, Gamow-Teller strengths, and NME decomposition for configurations of protons/neutrons pairs coupled to some spin (I) and some parity (positive or negative), called I-pair decomposition. These tests and validations of the SVD Hamiltonian can be found in [9] for ^{124}Sn and in [30] for ^{130}Te and ^{136}Xe. Calculations of NME in larger model spaces (e.g., $jj77$ model space that includes $0g_{9/2}$ and $0h_{9/2}$ orbitals missing in $jj55$ models space) were successfully performed for ^{136}Xe [31], but for ^{124}Sn and ^{130}Te they are much more difficult and would require special truncations.

In this work, assuming the detection of several tens of $0\nu\beta\beta$ decay events, we present a possibility to identify right-handed contributions from λ and η mechanisms by analyzing the two-electron angular and energy distributions that could be measured.

We organize this paper as follows: Section 2 shows a brief description of the neutrinoless double-beta decay formalism considering a low-energy Hamiltonian that takes into account contributions from right-handed currents. Section 3 presents an analysis of the half-lives and of the two-electron angular and energy distributions results for ^{124}Sn, ^{130}Te, and ^{136}Xe. Finally, we dedicate Section 4 to conclusions.

2. Brief Formalism of $0\nu\beta\beta$

The existence of right-handed currents and their contributions to the neutrinoless double-beta decay rate has been considered for a long time [14, 32], but most frequent calculations treat only the light left-handed neutrino-exchange mechanism (commonly referred to as "the mass mechanism"). One model that considers the right-handed currents contributions and includes heavy particles that are not part of the Standard Model is the left-right symmetric model [17, 18]. Within the framework of the left-right symmetric model, the neutrinoless double-beta decay half-life expression is

$$\left[T_{1/2}^{0\nu}\right]^{-1} = G_{01}^{0\nu} g_A^4 \left| M^{0\nu}\eta_\nu + M^{0N}\left(\eta_{N_R}^L + \eta_{N_R}^R\right) + \eta_\lambda X_\lambda + \eta_\eta X_\eta + \cdots \right|^2, \tag{1}$$

where $\eta_\nu, \eta_{N_R}^L, \eta_{N_R}^R, \eta_\lambda$, and η_η are neutrino physics parameters defined in [15] (see also Appendix A of [21]), $M^{0\nu}$ and M^{0N} are the light and heavy neutrino-exchange nuclear matrix elements [5, 6], and X_λ and X_η are combinations of NME and phase space factors, which are calculated in this paper. $G_{01}^{0\nu}$ is a phase space factor [33] that one can calculate [34] with good precision for most cases [35–37]. The "$\cdots$" sign represents other possible contributions, such as those of R-parity violating SUSY particle exchange [5, 6], Kaluza-Klein modes [6, 38, 39], violation of Lorentz invariance, and equivalence principle [40–42], which we neglected here. $\eta_{N_R}^L$ term also exists in the seesaw type I mechanisms but its contribution is negligible if the heavy mass eigenstates are larger than 1 GeV [8]. We consider a seesaw type I dominance [43] and we will neglect this contribution here.

For an easier read, we perform the following change of notation: $\langle\nu\rangle = |\eta_\nu|$, $\langle\lambda\rangle = |\eta_\lambda|$, and $\langle\eta\rangle = |\eta_\eta|$.

In this paper, we provide an analysis of the two-electron relative energy and angular distributions for ^{124}Sn, ^{130}Te, and ^{136}Xe using shell model NME that we calculate. The purpose of this analysis is to identify the relative contributions of η_λ and η_η terms in (1). A similar analysis for ^{82}Se was done using QRPA NME in [12] and with shell model NME in [21]. As in [21], we start from the classic paper of Doi et al. [14], describing the neutrinoless double-beta decay process using a low-energy effective Hamiltonian that includes the effects of the right-handed currents. By simplifying some notations and ignoring the contribution from $\eta_{N_R}^R$ term, which has the same energy and angular distribution as η_ν term, the half-life expression [14] is written as

$$\left[T_{1/2}^{0\nu}\right]^{-1} = \left|M_{\mathrm{GT}}^{0\nu}\right|^2 \left\{C_{\nu^2} + C_{\nu\lambda}\cos\phi_1 + C_{\nu\eta}\cos\phi_2 + C_{\lambda^2} + C_{\eta^2} + C_{\lambda\eta}\cos\left(\phi_1 - \phi_2\right)\right\}, \tag{2}$$

where ϕ_1 and ϕ_2 are the relative CP-violating phases (Eq. A7 of [21]) and $M_{\mathrm{GT}}^{0\nu}$ is the Gamow-Teller contribution of the light neutrino-exchange NME. C_α are contributions from different mechanisms: C_{ν^2} are from the left-handed leptonic currents, C_{λ^2} are from the right-handed leptonic and right-handed hadronic currents, and C_{η^2} are from the right-handed leptonic and left-handed hadronic currents. $C_{\nu\lambda}$, $C_{\nu\eta}$, and $C_{\lambda\eta}$ contain the interference between these terms. These are defined as

$$C_{\nu^2} = C_1 \langle\nu\rangle^2,$$

$$C_{\nu\lambda} = C_2 \langle\nu\rangle \langle\lambda\rangle,$$

$$C_{\nu\eta} = C_3 \langle\eta\rangle \langle\nu\rangle,$$

$$C_{\lambda^2} = C_4 \langle\lambda\rangle^2,$$

$$C_{\eta^2} = C_5 \langle \eta \rangle^2 ,$$
$$C_{\lambda\eta} = C_6 \langle \eta \rangle \langle \lambda \rangle , \tag{3}$$

where C_{1-6} are combinations of nuclear matrix elements and phase space factors (PSF). Their expressions can be found in Appendix B, Eqs. (B1) of [21]. $M^{0\nu}_{\mathrm{GT}}$ and the other nuclear matrix elements that appear in the expressions of the C_i factors are presented in Eq. (B4) of [21].

We write the differential decay rate for $0^+ \rightarrow 0^+$ $0\nu\beta\beta$ transition as

$$\frac{\mathrm{d}^2 W^{0\nu}_{0^+\rightarrow 0^+}}{\mathrm{d}\epsilon_1 \mathrm{d}\cos\theta_{12}} = \frac{a_{0\nu}\omega_{0\nu}(\epsilon_1)}{2(m_e R)^2}\left[A(\epsilon_1) + B(\epsilon_1)\cos\theta_{12}\right]. \tag{4}$$

Here, ϵ_1 is the energy of one electron in units of $m_e c^2$, R is the nuclear radius ($R = r_0 A^{1/3}$, with $r_0 = 1.2$ fm), θ_{12} is the angle between the outgoing electrons, and the expressions for the constant $a_{0\nu}$ and the function $\omega_{0\nu}$ are given in Appendix C, Eqs. (C2) and (C3) of [34], respectively. The functions $A(\epsilon)$ and $B(\epsilon)$ are defined as combinations of factors that include PSF and NME:

$$A(\epsilon_1) = |N_1(\epsilon_1)|^2 + |N_2(\epsilon_1)|^2 + |N_3(\epsilon_1)|^2 + |N_4(\epsilon_1)|^2 , \tag{5a}$$
$$B(\epsilon_1) = -2\,\mathrm{Re}\left[N_1^\star(\epsilon_1) N_2(\epsilon_1) + N_3^\star(\epsilon_1) N_4(\epsilon_1)\right]. \tag{5b}$$

The detailed expressions of $N_{1-4}(\epsilon_1)$ components are presented in Eqs. (B7) of [21].

We can express the half-life as follows:

$$\left[T^{0\nu}_{1/2}\right]^{-1} = \frac{1}{\ln 2}\int \mathrm{d}W^{0\nu}_{0^+\rightarrow 0^+} = \frac{a_{0\nu}}{\ln 2\,(m_e R)^2}\cdot\int_1^{T+1} A(\epsilon_1)\,\omega_{0\nu}(\epsilon_1)\,\mathrm{d}\epsilon_1, \tag{6}$$

with the normalized kinetic energy T defined as

$$T = \frac{Q_{\beta\beta}}{m_e c^2}, \tag{7}$$

where $Q_{\beta\beta}$ is the Q-value of the decay.

The integration of (4) over ϵ_1 provides the angular distribution of the electrons that we write as

$$\frac{\mathrm{d}W^{0\nu}_{0^+\rightarrow 0^+}}{\mathrm{d}\Omega} = \frac{a_{0\nu}}{4\pi(m_e R)^2}\left[\int_1^{T+1} A(\epsilon_1)\,\omega_{0\nu}(\epsilon_1)\,\mathrm{d}\epsilon_1 + \frac{\mathrm{d}\Omega}{2\pi}\int_1^{T+1} B(\epsilon_1)\,\omega_{0\nu}(\epsilon_1)\,\mathrm{d}\epsilon_1\right], \tag{8}$$

where $\mathrm{d}\Omega = 2\pi\mathrm{d}\cos\theta_{12}$.

Integrating (4) over $\cos\theta_{12}$ provides the single-electron spectrum. As in [21], we express the decay rate as a function of the difference in the energy of the two outgoing electrons: $\Delta t = (\epsilon_1 - \epsilon_2) m_e c^2$, where $\epsilon_2 = T + 2 - \epsilon_1$ is the kinetic energy of the second electron. We can write the energy of one electron as

$$\epsilon_1 = \frac{T + 2 + \Delta t/m_e c^2}{2}. \tag{9}$$

Changing the variable, the energy distribution as a function of Δt is

$$\frac{2\mathrm{d}W^{0\nu}_{0^+\rightarrow 0^+}}{\mathrm{d}(\Delta t)} = \frac{2a_{0\nu}}{(m_e R)^2}\frac{\omega_{0\nu}(\Delta t)}{m_e c^2}A(\Delta t). \tag{10}$$

Table 1: The nine NME of ^{124}Sn, ^{130}Te, and ^{136}Xe.

	M_{GT}	M_F	$M_{\mathrm{GT}\omega}$	$M_{F\omega}$	$M_{\mathrm{GT}q}$	M_{Fq}	M_T	M_R	M_P
^{124}Sn	1.85	−0.47	2.05	−0.46	1.79	−0.27	0.01	2.66	−2.06
^{130}Te	1.66	−0.44	1.86	−0.43	1.59	−0.25	−0.01	2.56	−1.73
^{136}Xe	1.50	−0.40	1.68	−0.39	1.44	−0.23	−0.01	2.34	−1.62

3. Results

The formalism used in this paper is taken from [21], where it was used to analyze the two-electron angular and energy distributions for ^{82}Se, the baseline isotope of the SuperNEMO experiment [12, 13]. It was adapted from [14, 33] with some changes for simplicity and consistency and updated with modern notations. Here we use it to analyze in detail $0\nu\beta\beta$ decay two-electron angular and energy distributions for ^{124}Sn, ^{130}Te, and ^{136}Xe. The nine NME required are calculated in this paper using the SVD shell model Hamiltonian [29] in $jj55$ model space which was thoroughly tested and validated for ^{124}Sn in [9] and for ^{130}Te and ^{136}Xe in [30]. For an easier comparison to other results, we use g_A value of 1.254; we include short-range correlations with CD-Bonn parametrization, finite nucleon size effects, and higher-order corrections of the nucleon current [44]. Should one change to the newer recommended g_A value of 1.27 [45], the NME results would change by only 0.5% [46] and the effective PSF (multiplied by g_A^4) would change by 5%. This is negligible when compared to the uncertainties in the NME. g_A quenching is not considered here and an extended justification for this decision is given in [21].

In Table 1, we present the nine dimensionless NME for ^{124}Sn, ^{130}Te, and ^{136}Xe calculated in this work using an optimal closure energy $\langle E \rangle = 3.5$ MeV which was obtained using a recently proposed method [47]. By using an optimal closure energy obtained for this Hamiltonian, we get $0\nu\beta\beta$ NME results in agreement with beyond closure approaches [48]. The definition of these NME and the details regarding their calculations are given in Appendix B of [21].

The integrated PSF of the outgoing electrons, denoted by G_1–G_9, which enter C_α terms of (2), depend on the Q-value of the transition, the mass, and the charge of the final nucleus. We calculate these integrated PSF using a new effective method [34] which was in agreement with the latest results and was tested for 11 nuclei. Their complete expressions can also be found in Appendix C of [21]. The largest difference between our PSF and those of [35], among our three isotopes

Table 2: The nine PSF expressed in [yr^{-1}].

	$G_1 \cdot 10^{14}$	$G_2 \cdot 10^{14}$	$G_3 \cdot 10^{14}$	$G_4 \cdot 10^{15}$	$G_5 \cdot 10^{13}$	$G_6 \cdot 10^{12}$	$G_7 \cdot 10^{10}$	$G_8 \cdot 10^{11}$	$G_9 \cdot 10^{11}$
^{124}Sn	1.977	4.184	1.248	3.909	6.685	3.648	2.749	2.585	0.731
^{130}Te	3.122	8.026	2.092	6.267	10.18	5.335	4.340	4.261	1.106
^{136}Xe	3.188	7.798	2.114	6.372	10.79	5.464	4.458	4.522	1.099

Table 3: C_i factors ($i = 1, \ldots, 6$) corresponding to (3) expressed in [yr^{-1}].

	$C_1 \cdot 10^{14}$	$C_2 \cdot 10^{14}$	$C_3 \cdot 10^{11}$	$C_4 \cdot 10^{13}$	$C_5 \cdot 10^{9}$	$C_6 \cdot 10^{13}$
^{124}Sn	2.67	−1.43	0.69	0.54	1.34	−0.71
^{130}Te	4.25	−2.41	1.08	1.64	2.26	−2.34
^{136}Xe	4.36	−2.44	1.30	1.04	2.24	−1.34

Table 4: The neutrino parameter values chosen for $0\nu\beta\beta$ mechanisms described in the text.

	$\langle\nu\rangle$	$\langle\lambda\rangle$	$\langle\eta\rangle$
Mass mechanism (ν)	$2 \cdot 10^{-7}$	0	0
Lambda mechanism (λ)	$2 \cdot 10^{-7}$	$2 \cdot 10^{-7}$	0
Eta mechanism (η)	$2 \cdot 10^{-7}$	0	$2 \cdot 10^{-9}$

Table 5: Calculated half-lives ($T_{1/2}$) intervals for each mechanism expressed in years. The range of the interval corresponds to the uncertainty in the CP phases ϕ_1 and ϕ_2 in (2).

	ν	λ	η
^{124}Sn	$2.73 \cdot 10^{26}$	$[7.41, 10.44] \cdot 10^{25}$	$[2.47, 4.69] \cdot 10^{25}$
^{130}Te	$2.12 \cdot 10^{26}$	$[5.07, 6.94] \cdot 10^{25}$	$[1.85, 3.34] \cdot 10^{25}$
^{136}Xe	$2.53 \cdot 10^{26}$	$[6.23, 8.60] \cdot 10^{25}$	$[2.20, 4.00] \cdot 10^{25}$

of interest, is of about 16% for G_8 of ^{136}Xe. Should one use the older formalism of [14], differences of about 88% are expected in the case of G_8 for ^{136}Xe. One should keep in mind that the expressions for the two-electron angular and energy distributions (A and B terms in (5a) and (5b)) contain energy-dependent (unintegrated) PSF and not the integrated PSF that are found in tables throughout the literature. Eqs. (B7) of [21] provide the details of their expressions. The values for the nine integrated PSF are presented in Table 2. The results shown include $g_A^4 = 1.254$ constant, such that $G_1 = G_{01}^{0\nu} g_A^4$ in (1) and $G_{[1,9]} = G_{[01,09]} g_A^4$ of [35].

C_i factors ($i = 1, \ldots, 6$) of (3), representing combinations of NME and PSF, are presented in Table 3. As one can clearly see, C_5 term that appears in η mechanism is the largest. This is because of the large magnitude of G_7, G_8, and G_9 PSF displayed in Table 2.

To test the possibility of disentangling the right-handed contributions in the framework of the left-right symmetric model, we consider three theoretical cases: the case of the mass mechanism denoted with ν and presented with the black color in the figures, the case of λ mechanism dominance in competition with ν denoted with λ and displayed with the blue color, and the case of η mechanism dominance in competition with ν denoted with η and displayed with the red color. This color choice is consistent throughout all the figures.

Considering the latest experimental limits [15, 35] from ^{76}Ge $0\nu\beta\beta$ half-life, we select a value for the mass mechanism parameter ν which corresponds to a light neutrino mass of about 1 meV, while the values for λ and η effective parameters are chosen to barely dominate over the mass mechanism. Should their values be reduced four times, their contributions would not be distinguishable from the mass mechanism. Table 4 shows the values of these parameters used in the analysis.

We consider four combinations for the CP phases ϕ_1 and ϕ_2 (each one being 0 or π) which can influence the half-lives and the two-electron distributions. The maximum difference arising from the interference of these phases produces the uncertainties that are displayed as bands in the figures, changing the amplitudes and the shapes. The color convention for Figures 2–9 assigns red bands with a wavy pattern (lighter grey in black and white print) to η mechanism and blue bands without a pattern (darker grey in black and white print) to λ mechanism. As the mass mechanism does not depend on ϕ_1 and ϕ_2, there is no interference, and it is represented by a single thick black line. Because the mass mechanism is the most studied case in the literature, one may consider it as the reference case.

The calculated half-lives of ^{124}Sn, ^{130}Te and ^{136}Xe are presented in Table 5. Their values can be obtained either from (2) or from (6). The maximum differences from the interference phases produce the intervals. For an easier comparison of the half-lives and the uncertainties, we also plot them in Figure 1. One can notice that the inclusion of λ or η contributions reduces the half-lives.

The shapes of the two-electron angular distributions of (8) could be used to distinguish between the mass mechanism and λ or η mechanisms. However, many recorded events (tens or more) are needed for a reliable evaluation, and even then one can face difficulties due to the unknown CP phases. ^{124}Sn angular distribution is presented in Figure 2. One can see that λ (blue bands) and η (red bands) exhibit similar shapes, differing in amplitude and opposite to that of the mass mechanism (black line). In the case of ^{130}Te, the same is to be expected, but λ and η bands overlap due to the unknown

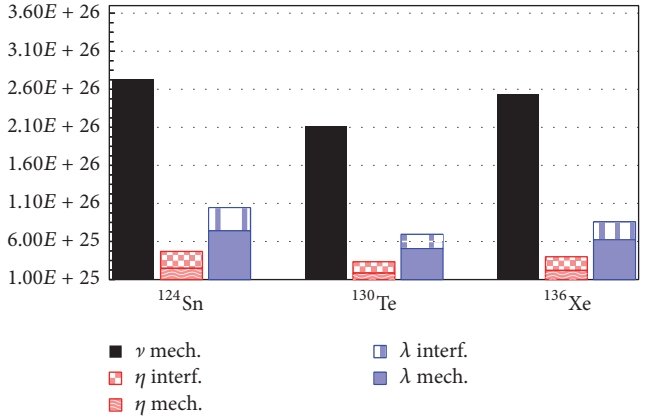

FIGURE 1: The calculated lifetimes and their uncertainties (the hatched bars) form the interference of the unknown CP phases. From left to right, the three vertical bars for each nucleus correspond to the mass mechanism, η mechanism, and λ mechanism, respectively.

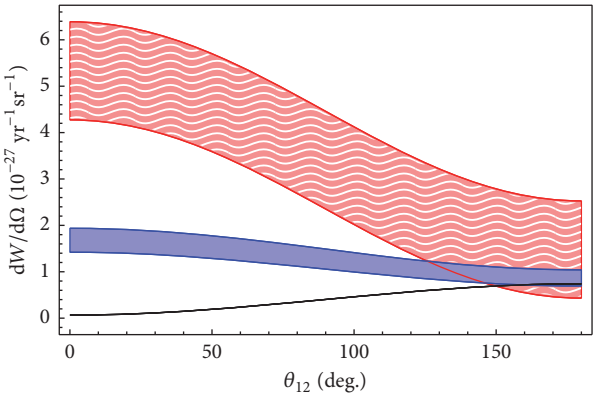

FIGURE 2: Electrons angular distribution for ^{124}Sn. The red band corresponds to η mechanism and the blue band corresponds to λ mechanism. The width of the bands represents the uncertainties arising from the unknown CP phases ϕ_1 and ϕ_2.

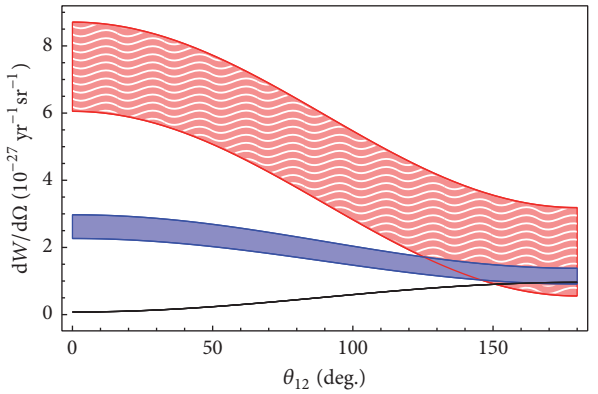

FIGURE 3: Same as Figure 2 for ^{130}Te.

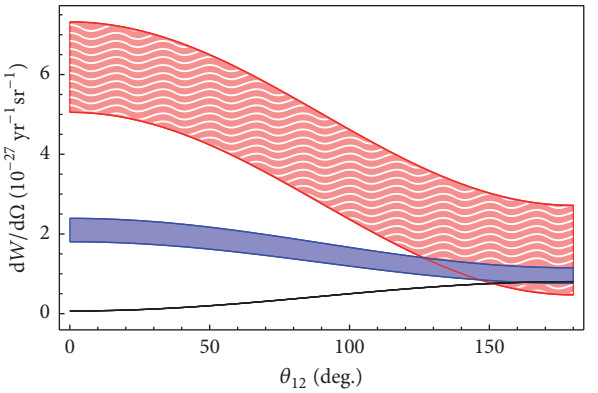

FIGURE 4: Same as Figure 2 for ^{136}Xe.

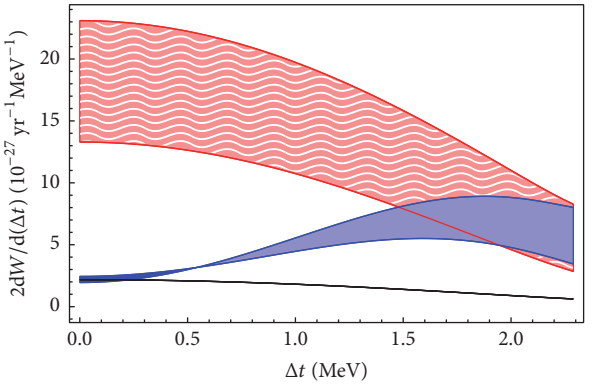

FIGURE 5: Electrons energy distribution for ^{124}Sn. The red band corresponds to η mechanism and the blue band corresponds to λ mechanism. The width of the bands represents the uncertainties arising from the unknown CP phases ϕ_1 and ϕ_2.

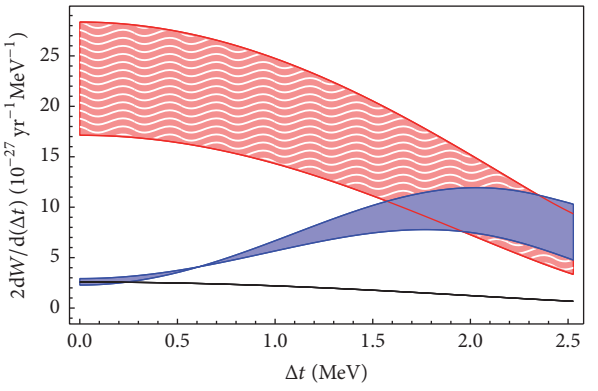

FIGURE 6: Same as Figure 5 for ^{130}Te.

phases, as seen in Figure 3. ^{136}Xe angular distribution is very similar to that of ^{124}Sn and is presented in Figure 4.

In principle, λ and η contributions could be identified in the shapes of the two-electron energy distributions. While the tails of the distributions (when the difference between the energy of one electron and that of the other is maximal) overlap, the starting points (when both electrons have almost

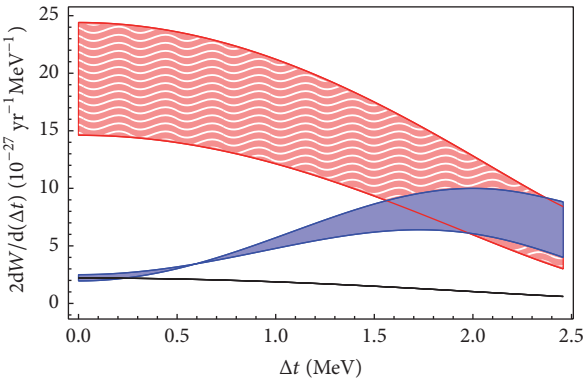

FIGURE 7: Same as Figure 5 for ^{136}Xe.

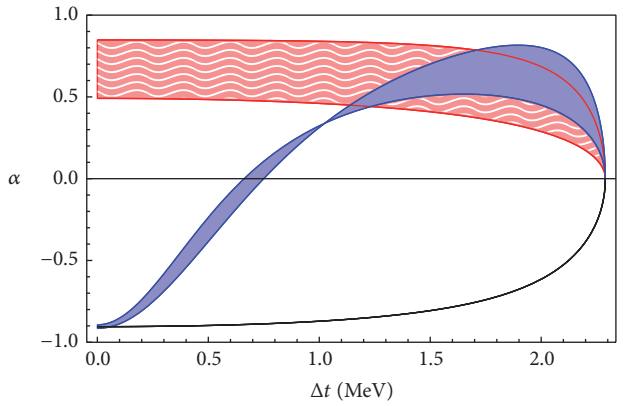

FIGURE 8: The angular correlation coefficient for ^{124}Sn. The red band corresponds to η mechanism and the blue band corresponds to λ mechanism. The width of the bands represents the uncertainties arising from the unknown CP phases ϕ_1 and ϕ_2.

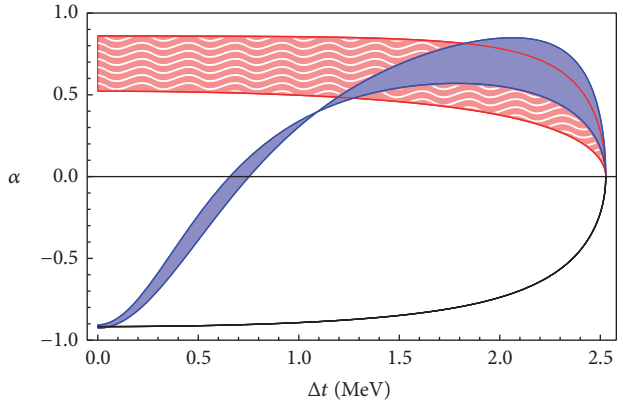

FIGURE 9: Same as Figure 8 for ^{130}Te.

equal energies) are very different for λ mechanism from η mechanism. Figure 5 shows the energy distribution for ^{124}Sn. ^{130}Te energy distribution is presented in Figure 6. For ^{136}Xe (Figure 7), we find an energy distribution very similar to that of ^{124}Sn, like in the case of the angular distributions.

To further aid with the disentanglement of λ and η mechanisms, we provide plots of the angular correlation

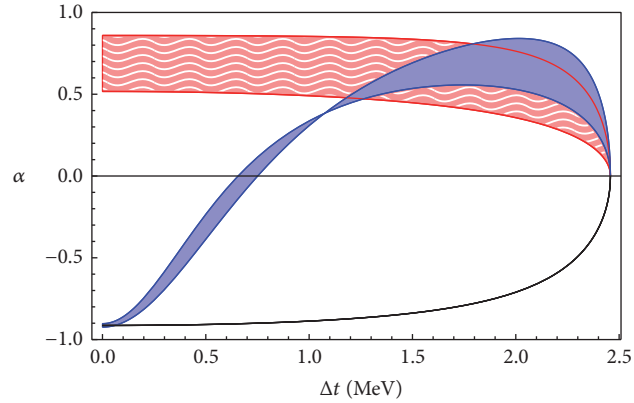

FIGURE 10: Same as Figure 8 for ^{136}Xe.

coefficient: $\alpha = B(\epsilon)/A(\epsilon)$ in our (4). This may help reduce the uncertainties induced by the unknown CP phases (see, e.g., Figures 6.5–6.9 of [14] and Figure 7 of [35]). From $\alpha(\Delta t)$, one may also obtain clearer separation from the mass mechanism over a wide range of energies. The angular correlation coefficient for ^{124}Sn is presented in Figure 8. The same behavior can be identified in Figure 9 for ^{130}Te and in Figure 10 for ^{136}Xe.

4. Conclusions

In this paper, we report shell model calculations necessary to disentangle the mixed right-handed/left-handed currents contributions (commonly referred to as η and λ mechanisms) from the mass mechanism in the left-right symmetric model. We perform an analysis of these contributions by considering three theoretical scenarios, one for the mass mechanism, one for λ dominance in competition with the mass mechanism, and one where η mechanism dominates in competition with the mass mechanism.

The figures presented support the conclusions [14, 21] that one can distinguish λ or η dominance over the mass mechanism from the shape of the two-electron angular distribution, while one can discriminate λ from η mechanism using the shape of the energy distribution and that of the angular coefficient. The tables and the figures presented also show the uncertainties related to the effects of interference from the unknown CP-violating phases.

We show our results for phase space factors, nuclear matrix elements, and lifetimes for $0\nu\beta\beta$ transitions of ^{124}Sn, ^{130}Te, and ^{136}Xe to ground states. In the case of the mass mechanism nuclear matrix elements, we obtain results which are consistent with previous calculations [21, 30], where the same SVD Hamiltonian was used. Similar to the case of ^{82}Se [21], the inclusion of η and λ mechanisms contributions tends to decrease the half-lives.

The phase space factors included in the analysis of lifetimes and two-electron distributions are calculated using a recently proposed accurate effective method [9] that provides results very close to those of [35]. Reference [35] takes into account consistently the effects of the realistic finite size

proton distribution in the daughter nucleus, but it does not provide all the energy-dependent phase space contributions necessary for our analysis.

Consistent with the calculations and the conclusions we obtained for ^{82}Se [21], if η mechanism exists, it may be favored to compete with the mass mechanisms because of the larger contribution from the phase space factors.

Finally, we conclude that, in experiments where outgoing electrons can be tracked, such as SuperNEMO [12, 13] and NEXT [49], this analysis is possible if enough data is collected, generally of the order of a few tens of events. This may be beyond the capabilities of some of the current experiments, but should a positive neutrinoless double-beta decay measurement be achieved, it is expected that more resources could be allocated to improve the design, the statistics, and the variety of the investigated isotopes of the experiments which have realistic tracking capabilities.

Competing Interests

The authors declare that they have no competing interests.

Acknowledgments

Support from the NUCLEI SciDAC Collaboration under US Department of Energy (Grant no. DE-SC0008529) is acknowledged. Mihai Horoi also acknowledges US NSF, Grant no. PHY-1404442, and US Department of Energy, Grant no. DE-SC0015376.

References

[1] J. Schechter and J. W. F. Valle, "Neutrinoless double- decay in SU(2)×U(1) theories," *Physical Review D*, vol. 25, no. 11, pp. 2951–2954, 1982.

[2] J. Nieves, "Dirac and pseudo-Dirac neutrinos and neutrinoless double beta decay," *Physics Letters B*, vol. 147, no. 4-5, pp. 375–379, 1984.

[3] E. Takasugi, "Can the neutrinoless double beta decay take place in the case of Dirac neutrinos?" *Physics Letters B*, vol. 149, no. 4-5, pp. 372–376, 1984.

[4] M. Hirsch, S. Kovalenko, and I. Schmidt, "Extended Black box theorem for lepton number and flavor violating processes," *Physics Letters B*, vol. 642, no. 1-2, pp. 106–110, 2006.

[5] J. D. Vergados, H. Ejiri, and F. Šimkovic, "Theory of neutrinoless double-beta decay," *Reports on Progress in Physics*, vol. 75, no. 10, Article ID 106301, 2012.

[6] M. Horoi, "Shell model analysis of competing contributions to the double-β decay of ^{48}Ca," *Physical Review C*, vol. 87, no. 1, Article ID 014320, 2013.

[7] M. Mitra, G. Senjanović, and F. Vissani, "Neutrinoless double beta decay and heavy sterile neutrinos," *Nuclear Physics B*, vol. 856, no. 1, pp. 26–73, 2012.

[8] M. Blennow, E. Fernandez-Martinez, J. Lopez-Pavon, and J. Menendez, "Neutrinoless double beta decay in seesaw models," *Journal of High Energy Physics*, vol. 2010, no. 7, article 096, 2010.

[9] M. Horoi and A. Neacsu, "Shell model predictions for ^{124}Sn double-β decay," *Physical Review C*, vol. 93, no. 2, Article ID 024308, 2016.

[10] J. D. Holt and J. Engel, "Effective double-β-decay operator for ^{76}Ge and ^{82}Se," *Physical Review C*, vol. 87, no. 6, Article ID 064315, 2013.

[11] J. Retamosa, E. Caurier, and F. Nowacki, "Neutrinoless double beta decay of Ca48," *Physical Review C*, vol. 51, no. 1, pp. 371–378, 1995.

[12] R. Arnold, C. Augier, J. Baker et al., "Probing new physics models of neutrinoless double beta decay with SuperNEMO," *The European Physical Journal C*, vol. 70, no. 4, pp. 927–943, 2010.

[13] M. Bongrand, "Search for $0\nu2\beta$ of ^{100}Mo by NEMO-3 and status of SuperNEMO," in *Proceedings of the 26th International Conference on Neutrino Physics and Astrophysics: Neutrino*, vol. 1666 of *AIP Conference Proceedings*, Boston, Mass, USA, June 2014.

[14] M. Doi, T. Kotani, and E. Takasugi, "Double beta decay and Majorana neutrino," *Progress of Theoretical Physics Supplement*, vol. 83, pp. 1–175, 1985.

[15] J. Barry and W. Rodejohann, "Lepton number and flavour violation in TeV-scale left-right symmetric theories with large left-right mixing," *Journal of High Energy Physics*, vol. 2013, no. 9, article 153, 2013.

[16] J. C. Pati and A. Salam, "Lepton number as the fourth 'color'," *Physical Review D*, vol. 10, no. 1, pp. 275–289, 1974.

[17] R. N. Mohapatra and J. C. Pati, "'Natural' left-right symmetry," *Physical Review D*, vol. 11, no. 9, pp. 2558–2561, 1975.

[18] G. Senjanovic and R. N. Mohapatra, "Exact left-right symmetry and spontaneous violation of parity," *Physical Review D*, vol. 12, no. 5, pp. 1502–1505, 1975.

[19] W.-Y. Keung and G. Senjanovic, "Majorana neutrinos and the production of the right-handed charged Gauge Boson," *Physical Review Letters*, vol. 50, no. 19, article 1427, 1983.

[20] V. Khachatryan, A. M. Sirunyan, A. Tumasyan et al., "Search for heavy neutrinos and W bosons with right-handed couplings in proton-proton collisions at $\sqrt{s} = 8$ TeV," *The European Physical Journal C*, vol. 74, no. 11, article 3149, pp. 1–23, 2014.

[21] M. Horoi and A. Neacsu, "Analysis of mechanisms that could contribute to neutrinoless double-beta decay," *Physical Review D*, vol. 93, no. 11, Article ID 113014, 2016.

[22] V. Nanal, "Search for neutrinoless double beta decay in 124Sn," in *Proceedings of the International Nuclear Physics Conference (INPC '13)*, vol. 66 of *EPJ Web of Conferences*, p. 08005, March 2014.

[23] K. Alfonso, D. R. Artusa, F. T. Avignone et al., "Search for neutrinoless double-β decay of ^{130}Te with CUORE-0," *Physical Review Letters*, vol. 115, no. 10, Article ID 102502, 2015.

[24] C. Alduino, K. Alfonso, D. R. Artusa et al., "CUORE-0 detector: design, construction and operation," *Journal of Instrumentation*, vol. 11, no. 7, pp. 1–35, 2016.

[25] S. Andringa, E. Arushanova, S. Asahi et al., "Current status and future prospects of the SNO+ experiment," *Advances in High Energy Physics*, vol. 2016, Article ID 6194250, 21 pages, 2016.

[26] J. J. Gomez-Cadenas, V. Álvarez, F. I. G. Borges et al., "Present status and future perspectives of the NEXT experiment," *Advances in High Energy Physics*, vol. 2014, Article ID 907067, 22 pages, 2014.

[27] J. B. Albert, D. J. Auty, P. S. Barbeau et al., "Search for Majorana neutrinos with the first two years of EXO-200 data," *Nature*, vol. 510, no. 7504, pp. 229–234, 2014.

[28] A. Gando, Y. Gando, T. Hachiya et al., "Search for Majorana neutrinos near the inverted mass Hierarchy region with KamLAND-Zen," *Physical Review Letters*, vol. 117, no. 8, Article ID 082503, 6 pages, 2016.

[29] C. Qi and Z. X. Xu, "Monopole-optimized effective interaction for tin isotopes," *Physical Review C*, vol. 86, no. 4, Article ID 044323, 11 pages, 2012.

[30] A. Neacsu and M. Horoi, "Shell model studies of the ^{130}Te neutrinoless double-β decay," *Physical Review C*, vol. 91, no. 2, Article ID 024309, 9 pages, 2015.

[31] M. Horoi and B. A. Brown, "Shell-model analysis of the ^{136}Xe double beta decay nuclear matrix elements," *Physical Review Letters*, vol. 110, no. 22, Article ID 222502, 2013.

[32] M. Doi, T. Kotani, H. Nishiura, and E. Takasugi, "Double beta decay," *Progress of Theoretical Physics*, vol. 69, no. 2, pp. 602–635, 1983.

[33] J. Suhonen and O. Civitarese, "Weak-interaction and nuclear-structure aspects of nuclear double beta decay," *Physics Report*, vol. 300, no. 3-4, pp. 123–214, 1998.

[34] M. Horoi and A. Neacsu, "An effective method to accurately calculate the phase space factors for $\beta^-\beta^-$ decay," *Advances in High Energy Physics*, vol. 2016, Article ID 7486712, 8 pages, 2016.

[35] D. Štefánik, R. Dvornický, F. Šimkovic, and P. Vogel, "Reexamining the light neutrino exchange mechanism of the $0\nu\beta\beta$ decay with left- and right-handed leptonic and hadronic currents," *Physical Review C*, vol. 92, no. 5, Article ID 055502, 2015.

[36] J. Kotila and F. Iachello, "Phase-space factors for double-β decay," *Physical Review C*, vol. 85, no. 3, Article ID 034316, 2012.

[37] S. Stoica and M. Mirea, "New calculations for phase space factors involved in double-β decay," *Physical Review C*, vol. 88, no. 3, Article ID 037303, 2013.

[38] G. Bhattacharyya, H. V. Klapdor-Kleingrothaus, H. Pas, and A. Pilaftsis, "Neutrinoless double beta decay from singlet neutrinos in extra dimensions," *Physical Review D*, vol. 67, no. 11, Article ID 113001, 2003.

[39] F. Deppisch and H. Päs, "Pinning down the mechanism of neutrinoless double β decay with measurements in different nuclei," *Physical Review Letters*, vol. 98, no. 23, Article ID 232501, 4 pages, 2007.

[40] C. N. Leung, "Neutrino tests of general and special relativity," *Nuclear Instruments and Methods in Physics Research A*, vol. 451, no. 1, pp. 81–85, 2000.

[41] H. Klapdor-Kleingrothaus, H. Päs, and U. Sarkar, "Test of special relativity and equivalence principle from neutrinoless double beta decay," *The European Physical Journal A—Hadrons and Nuclei*, vol. 5, no. 1, pp. 3–6, 1999.

[42] G. Barenboim, J. Beacom, L. Borissov, and B. Kayser, "CPT violation and the nature of neutrinos," *Physics Letters B*, vol. 537, no. 3-4, pp. 227–232, 2002.

[43] P. S. Bhupal Dev, S. Goswami, and M. Mitra, "TeV-scale left-right symmetry and large mixing effects in neutrinoless double beta decay," *Physical Review D*, vol. 91, no. 11, Article ID 113004, 2015.

[44] M. Horoi and S. Stoica, "Shell model analysis of the neutrinoless double-β decay of ^{48}Ca," *Physical Review C*, vol. 81, no. 2, Article ID 024321, 7 pages, 2010.

[45] K. A. Olive, K. Agashe, C. Amsler et al., "Review of particle physics," *Chinese Physics C*, vol. 38, no. 9, Article ID 090001, 2014.

[46] R. A. Sen'kov, M. Horoi, and B. A. Brown, "Neutrinoless double-β decay of ^{82}Se in the shell model: beyond the closure approximation," *Physical Review C*, vol. 89, no. 5, Article ID 054304, 7 pages, 2014.

[47] R. A. Sen'kov and M. Horoi, "Accurate shell-model nuclear matrix elements for neutrinoless double-β decay," *Physical Review C*, vol. 90, no. 5, Article ID 051301, 2014.

[48] R. A. Sen'kov and M. Horoi, "Neutrinoless double-β decay of ^{48}Ca in the shell model: closure versus nonclosure approximation," *Physical Review C*, vol. 88, no. 6, Article ID 064312, 2013.

[49] S. Cebrián, J. Pérez, I. Bandac et al., "Radiopurity assessment of the tracking readout for the NEXT double beta decay experiment," *Journal of Instrumentation*, vol. 10, Article ID P05006, 2015.